

Coalescing of geostrophic vortices

By R. W. GRIFFITHS

Research School of Earth Sciences, Australian National University, GPO Box 4, Canberra,
A.C.T. 2601, Australia.

AND E. J. HOPFINGER

Institut de Mecanique, Laboratoire Associé au C.N.R.S., Université de Grenoble, B.P. 68,
38402 St. Martin d'Heres, France.

Close interactions between pairs of two-dimensional vortices of like sign were investigated in experiments with barotropic vortices and baroclinic vortices. The vortices were generated by sources or sinks in a rotating fluid which, respectively, was homogeneous or contained a two-layer density stratification. For two identical anticyclonic, unstratified vortices there was a critical separation distance beyond which the vortices coalesced to form a single larger anticyclone. The critical distance d_* , scaled by the radius R of a core having non-zero relative vorticity, was $d_*/R = 3.3 \pm 0.2$. This value is in agreement with results of previous numerical simulations for finite-area vortices in non-rotating flows. The effects on vortex structure of Ekman pumping due to the presence of a rigid boundary caused cyclonic vortices to coalesce from larger distances. Baroclinic vortices in a two-layer stratification were also found to coalesce despite a potential-energy barrier. However, the critical separation distance depended on the internal Rossby radius. When the Rossby radius was large compared with the core radius, vortices coalesced from distances much greater than the critical distance for barotropic vortices. Coalescing of two vortices of equal size and strength led to two symmetric entwined spirals of water, while close interaction of unequal vortices caused the weaker vortex to be wrapped around the outer edge of the stronger. Implications of these results are discussed for ocean eddies and intense atmospheric cyclones.

1. Introduction

Numerical simulations using the Euler equations have shown that inviscid two-dimensional vortices with finite cores of anomalous vorticity will coalesce when the distance d between vortex centres is sufficiently small (Christiansen 1973; Christiansen & Zabusky 1973; Overman & Zabusky 1982). For two identical Rankine vortices (which have cores of uniform vorticity) embedded in a fluid with no background rotation and no density gradients the numerical studies indicate that the critical separation is $d_*/R \approx 3.2$, where R is the core radius (although the exact value of d_*/R depends to some extent upon the nature of the imposed perturbation and the initial shape assumed for the vortices – Overman & Zabusky 1982; Dritschel 1985). At separation distances smaller than the critical value the velocity field induced by each vortex causes the finite core of the other to become increasingly distorted, until each core is drawn out and advected around the other. At larger separations the cores may experience some oscillatory perturbations but remain separate (Overman & Zabusky 1982). The process of coalescing has been termed ‘convective merging’ (Rossow 1977) or vortex ‘pairing’, the latter description originating in observations of the cascade of pair-wise interactions of vortices in

unstable shear layers. 'Pairing' of two-dimensional vortices is responsible for the growth of mixing layers (Winant & Browand 1974; Brown & Roshko 1974) and is observed in the later stages of the development of Kelvin-Helmholtz billows (Thorpe 1973). The application of point-vortex methods to simulate vortex interactions has been reviewed by Aref (1983). However, apart from the experiments with trains of vortices, as in shear layers, there have been few laboratory investigations of the close interactions between two-dimensional vortices. Fujiwhara (1923) attempted to model the behaviour of hurricane pairs using two cyclonic vortices in an unstratified rotating tank, while P. Caperan & T. Maxworthy (private communication) recently observed interactions of barotropic vortices generated by moving flaps in a non-rotating tank.

In recent laboratory experiments aimed at studying the combined influence of background (or planetary) rotation and density stratification on the interactions of vortex dipoles (Griffiths & Hopfinger 1986) it was noticed that vortices of the same sign and in the same layer of a two-layer stratification sometimes coalesced. Coalescing took place when the baroclinic vortices were brought close together by the advective velocities induced by all other vortices in the container. It occurred most often when the internal Rossby radius of deformation was large. Evolution of the flow then deviated from that predicted by treating each vortex as a point vortex moving passively with the ambient-fluid velocity (Hogg & Stommel 1985).

Eddies in oceans and atmospheres are strongly influenced by vertical density gradients in the fluid. Hence interactions of baroclinic geostrophic vortices are of interest both in studies of the dynamics of individual eddy collisions and for their contribution to the dynamics of geostrophic turbulence. However, the conditions under which eddies (i.e. vortices with finite cores) in a stratified rotating fluid will coalesce have not been investigated. Calculations of the energy of the flow in an ageostrophic model for an eddy with finite radius, including centrifugal forces (Gill & Griffiths 1981), show that if the potential vorticity of the fluid is conserved both the potential energy and the total energy of the flow must increase when two eddies coalesce into one. In this model the depth of one layer (the fluid within the eddies) is constrained to vanish on the perimeter of each eddy (a model for eddies formed by instability at oceanic density fronts, Flierl 1979), so that velocities are zero outside the eddies and each eddy possesses a well-defined total energy. These we refer to as isolated frontal eddies. We conclude that coalescing of such eddies would require either an external energy source or an alteration of the potential vorticity in the eddies. Quasi-geostrophic eddies, on the other hand, where the eddies induce small vertical displacements of density surfaces, are not isolated as the flow has a velocity which decays at large distances as the inverse of the distance from the eddy centre. Such eddies involve a finite potential energy but an unbounded kinetic energy (if in a horizontally unbounded container), as is shown clearly by the point-vortex model of Hogg & Stommel (1985). However, the point-vortex model shows that if potential vorticity is conserved, the potential energy of the flow must again increase as two vortices of the same sign approach each other. In this case there could be a conversion of kinetic to potential energy and it is not clear that either an external energy supply or alteration of potential vorticity is necessary for coalescing to be possible.

The above energy calculations do suggest that merging of baroclinic vortices might be less likely than it would be for unstratified barotropic vortices. On the other hand, it is conceivable that dissipation of potential vorticity is essential, or that the total volume of the rotational core after a merger is not equal to the sum of the volumes of the initial vortex cores, so that merging of baroclinic vortices becomes possible. Of interest here are Dritschel's (1985) conclusions for finite-area *barotropic* vortices:

under some circumstances two vortices can undergo an inviscid merger into a 6:1 ellipse, but a very small amount of dissipation greatly reduces constraints on merging and allows coalescing to proceed under a much broader range of conditions. On this same point, Pierrehumbert & Widnall (1981) show that conservation of vorticity during merger of unstratified shear-layer vortices would imply an increase of energy, and conclude that coalescence must in general involve entrainment of irrotational fluid.

Very few examples of coalescing have been documented for ocean eddies. The paucity of observations might be a result of a real scarcity of merging events, in turn due to an inability of baroclinic eddies to coalesce without sufficient energy input, or might simply reflect the practical difficulties encountered in observing, sampling and interpreting oceanic flow. Nevertheless, one clear example of coalescing of two large warm eddies shed by the East Australia Current was recorded in some detail (Cresswell 1982). In the atmosphere, intense tropical cyclones sometimes form in pairs and proceed to orbit around a mutual centre of vorticity (Brand 1970). In this case we have found no record of coalescing, although hurricane pairs with separations of less than 750 km show a tendency to attract each other.

In this paper we present the results of experiments in which two vortices of the same sign, with known strengths and vorticity structure, were generated at desired separation distances in a rotating container and subsequently left to interact. Both unstratified and baroclinic (two-layer) vortices were investigated. We consider the roles of the core radius and Rossby radius in the vortex interactions. Rossby numbers for the flow within individual vortices were similar to those for ocean eddies and the results are compared with the recorded merging of eddies 'Leo' and 'Maria' in the Tasman Sea.

2. Laboratory apparatus and technique

The apparatus and method for generating vortices were described in Griffiths & Hopfinger (1986). Briefly, experiments were carried out in a circular tank 100 cm in diameter, 45 cm deep and rotating about a vertical axis through its centre. In most experiments the rotation rate was $\Omega = 1.0 \text{ rads}^{-1}$ in the anticlockwise direction. One rotation period was then $T_\Omega = 2\pi\Omega^{-1} = 6.28 \text{ s}$ and the background vorticity was $f = 2.0 \text{ s}^{-1}$. Video, 35 mm and cine cameras mounted above the tank in the rotating reference frame recorded the patterns of injected dye and motions of floating or neutrally buoyant particles.

When no stratification was required the tank was filled to a depth of either 20 cm or 40 cm with fresh water at room temperature. The water was spun up to a state of solid-body rotation before an experiment was begun. When a two-layer stratification was required a layer of fresh water 20 cm deep was spun up and a sugar solution fed slowly onto the bottom through a tube at the wall. Once both layers were of equal depth the water was left to slowly approach solid-body rotation, although this state was never fully reached as diffusion of solute continued to drive a slow persistent azimuthal flow of the character described by Griffiths & Linden (1985). Vertical traverses with a conductivity probe in several experiments, where sugar was replaced by salt, showed that the density interface was approximately 2 cm thick. Despite great care during the filling procedure thinner interfaces could not be achieved, and we note that the conductivity profiles were essential since the interface appeared to the naked eye as though it was only a few millimetres thick. The internal Rossby radii $\lambda = (g\Delta\rho H/\rho)^{1/2}f^{-1}$, based on the layer depth $H = 20 \text{ cm}$ and the Coriolis

parameter $f = 2 \text{ s}^{-1}$, were $\lambda = 1.5, 5, 10$ and 15 cm . The unstratified case corresponds to the limit of vanishing Rossby radius.

Each vortex was generated by a source (an anticyclone) or a sink (a cyclone) at the free surface of the water. These were tubes 3 cm in diameter and filled with permeable foam. Tubes of smaller diameter were sometimes used as sinks, but the behaviour of the vortices showed no dependence on the form of sink used. Flow through the sources and sinks was driven by constant-gravitational heads and controlled using flowmeters in the non-rotating reference frame. Water supplied to sources was of the same temperature and density as the upper layer in the tank.

When generating two vortices of the same sign the sources (or sinks) were positioned a desired distance d apart and were symmetric about the centre of the tank. The latter precaution was intended to minimize effects of the sidewall and the slow persistent anticyclonic flow in the top layer. Flow through the sources (or sinks) was turned on for a fixed period of 30 s , which is close to $5T_\Omega$. During forcing dye of different colours could be injected into the cores of the developing vortices. This dye served as a ready guide to the subsequent position and shape of the vortex, as well as labelling the water initially within each vortex. As the forcing was turned off digital clocks reading elapsed time in rotation periods (to $0.1T_\Omega$) were started from zero. The dye showed that the flow was always independent of depth within each layer of uniform density.

The distribution of horizontal velocity was obtained from time exposures showing the horizontal paths of neutrally buoyant beads. The beads were illuminated by a horizontal sheet of light 2 cm thick directed alternately through the mid-depth of the top layer and the mid-depth of the bottom layer. In unstratified cases the sheet of light was approximately 10 cm above the bottom.

3. Vortex structure

3.1. *A model baroclinic vortex*

Baroclinic vortices are characterized by two horizontal length-scales that are generally independent: the Rossby radius of deformation and a core radius. A simple model of a two-layer geostrophic vortex is shown in figure 1. Both layers are assumed to have equal 'rest' depths H . The fluid having anomalous potential vorticity is confined to the upper layer and forms the vortex core of radius R . The core has a uniform potential vorticity Π_0 , different from the potential vorticity $\Pi = f/H$ of the remainder of the fluid. Since $\Pi = (f + \zeta)/\eta$, where ζ is the relative vorticity and η the height of the column of unstratified fluid, fluid outside the core would have zero relative vorticity only if the layer depth locally was equal to H . This model vortex structure is more simple than that expected for oceanic or atmospheric vortices, where the potential vorticity may not be entirely uniform within the core, the density varies continuously with depth, and fractional variations of layer depth (in oceanic frontal eddies) can be large. However, the model does capture the basic features of the real flow.

For anticyclonic laboratory vortices produced by sources, the injected water has little angular momentum ($\zeta \approx -f$) and we expect cores with small potential vorticity ($\Pi_0 \ll f/H$). The core size is determined largely by the volume injected. For cyclonic vortices generated by sinks, the initial size and structure of the core are determined by the diameter of the sink and horizontal diffusion of momentum. Positive relative vorticity is created by local stretching of fluid columns as they are drawn into the

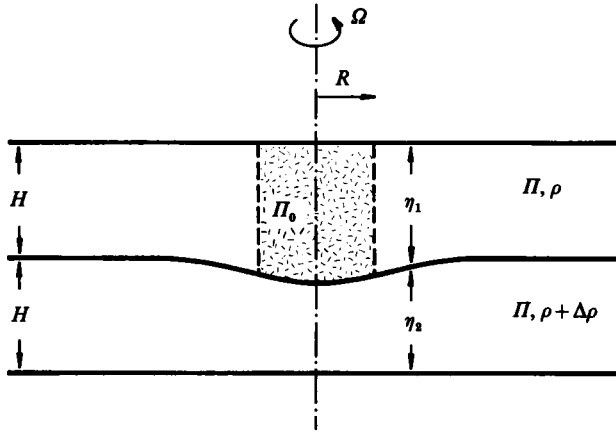


FIGURE 1. A diagram of the model two-layer geostrophic vortex with piecewise uniform potential vorticity.

sink. However, once the forcing is cut off there is no further stretching of columns (apart from that due to motion of the density interface). The potential vorticity is then given by the layer depth η ($\approx H$) and the relative vorticity ζ induced during the forcing period. Thus Π is large near the sink ($\Pi_0 > f/H$) but uniform and equal to f/H elsewhere. Neglecting effects of Ekman suction, the bottom layer must have uniform potential vorticity $\Pi = f/H$ so long as the interface is not drawn up into the sink.

In the model the flow is assumed to satisfy the inviscid quasi-geostrophic potential-vorticity equations (Pedlosky 1979):

$$\left. \begin{aligned} \nabla^2 \psi_a + \frac{1}{2} \lambda^{-2} (\psi_b - \psi_a) &= H \Pi_0 - f, & r < R, \\ \nabla^2 \psi_a + \frac{1}{2} \lambda^{-2} (\psi_b - \psi_a) &= 0, & r > R, \\ \nabla^2 \psi_b + \frac{1}{2} \lambda^{-2} (\psi_a - \psi_b) &= 0, \end{aligned} \right\} \quad (1)$$

where subscripts a and b refer to the top and bottom layer, respectively, ψ is a stream function and $\lambda = (g'H)^{1/2}/f$, with $g' = g\Delta\rho/\rho$, is the Rossby radius. The right-hand side of (1) is simply the relative vorticity $\zeta = H\Pi - f$, which vanishes everywhere outside the core. Within the core a potential vorticity $\Pi_0 = 0$ (as would be achieved by injecting water from a line source at $r = 0$) implies a relative vorticity $\zeta_0 = -f$, while $\zeta_0 = f$ corresponds to $\Pi_0 = 2f/H$.

In polar coordinates centred at $r = 0$, an axisymmetric vortex has azimuthal velocities $v_a = \partial\psi_a/\partial r$ and $v_b = \partial\psi_b/\partial r$. Suitable boundary conditions on the solution to (1) are

$$\left. \begin{aligned} \frac{\partial\psi_a}{\partial r} = \frac{\partial\psi_b}{\partial r} &= 0, & r = 0, \\ \frac{\partial\psi_a}{\partial r} \rightarrow \frac{\partial\psi_b}{\partial r} &\rightarrow 0, & r \rightarrow \infty, \\ \psi_b &= 0, & r = 0, \\ \psi_a, \psi_b, \frac{\partial\psi_a}{\partial r}, \frac{\partial\psi_b}{\partial r} &\text{ continuous at } r = R. \end{aligned} \right\} \quad (2)$$

The bottom is taken to be an isopotential surface and the interface height is given by

$$\eta_2 = H + \frac{f}{g}(\psi_a - \psi_b), \quad (3)$$

which is continuous by virtue of the continuity of the stream functions.

A quasi-geostrophic model similar to that formulated above is presented for point vortices by Gryanik (1983) and Hogg & Stommel (1985), in which case each vortex is represented as a delta function in potential vorticity in one of the two layers. The quasi-geostrophic assumption neglects local accelerations ($\partial \mathbf{u} / \partial t$) relative to coriolis accelerations ($2\boldsymbol{\Omega} \times \mathbf{u}$), and takes the relative vorticity to be comparable with vorticity associated with stretching of fluid columns by variations in layer depth, but small compared with the background vorticity f . While departures from exact geostrophic balance are allowed, the model does not include the centrifugal forces v^2/r that are associated with finite Rossby numbers ζ/f and which are significant in frontal ocean eddies (Flierl 1979). †

Solutions to (1) are found by addition and subtraction of equations for the top and bottom layers in each of the regions $r \leq R$. The resulting solutions for $\psi_a + \psi_b$ and $\psi_a - \psi_b$ are then recombined to find

$$\left. \begin{aligned} \psi_a &= a - \frac{1}{2}\lambda^2\zeta_0 + \frac{1}{8}\zeta_0 r^2 + b \ln r + cI_0\left(\frac{r}{\lambda}\right) + dK_0\left(\frac{r}{\lambda}\right) \\ \psi_b &= a + \frac{1}{2}\lambda^2\zeta_0 + \frac{1}{8}\zeta_0 r^2 + b \ln r - cI_0\left(\frac{r}{\lambda}\right) - dK_0\left(\frac{r}{\lambda}\right) \end{aligned} \right\} r < R, \quad (4)$$

$$\left. \begin{aligned} \psi_a &= \alpha + \beta \ln r + \gamma I_0\left(\frac{r}{\lambda}\right) + \delta K_0\left(\frac{r}{\lambda}\right) \\ \psi_b &= \alpha + \beta \ln r - \gamma I_0\left(\frac{r}{\lambda}\right) - \delta K_0\left(\frac{r}{\lambda}\right) \end{aligned} \right\} r > R,$$

where $a, b, c, d, \alpha, \beta, \gamma$ and δ are constants. Applying the conditions (2) the vortex stream functions become ‡

$$\left. \begin{aligned} \frac{\psi_a}{\lambda^2\zeta_0} &= -1 + \frac{1}{8}\frac{r^2}{\lambda^2} + \frac{1}{2}\frac{R}{\lambda}K_1\left(\frac{R}{\lambda}\right)\left[1 + I_0\left(\frac{r}{\lambda}\right)\right] \\ \frac{\psi_b}{\lambda^2\zeta_0} &= \frac{1}{8}\frac{r^2}{\lambda^2} + \frac{1}{2}\frac{R}{\lambda}K_1\left(\frac{R}{\lambda}\right)\left[1 - I_0\left(\frac{r}{\lambda}\right)\right] \end{aligned} \right\} r < R, \quad (5)$$

$$\left. \begin{aligned} \frac{\psi_a}{\lambda^2\zeta_0} &= -\frac{1}{2} + \frac{1}{4}\frac{R^2}{\lambda^2}\left(\frac{1}{2} + \ln \frac{r}{R}\right) + \frac{1}{2}\frac{R}{\lambda}\left[K_1\left(\frac{R}{\lambda}\right) - I_1\left(\frac{R}{\lambda}\right)K_0\left(\frac{r}{\lambda}\right)\right] \\ \frac{\psi_b}{\lambda^2\zeta_0} &= -\frac{1}{2} + \frac{1}{4}\frac{R^2}{\lambda^2}\left(\frac{1}{2} + \ln \frac{r}{R}\right) + \frac{1}{2}\frac{R}{\lambda}\left[K_1\left(\frac{R}{\lambda}\right) + I_1\left(\frac{R}{\lambda}\right)K_0\left(\frac{r}{\lambda}\right)\right] \end{aligned} \right\} r > R.$$

† Another model in which the momentum equation is approximated by an exact geostrophic balance but in which the exact equation for conservation of potential vorticity is used, is readily solved for the flow of figure 1 and yields velocity profiles of the same form as those derived in this paper. However, that model, too, neglects effects of finite Rossby number.

‡ These expressions make use of the identity $I_1(x)K_0(x) + I_0(x)K_1(x) = 1/x$, where I_n, K_n are the modified Bessel functions.

The corresponding azimuthal velocities are

$$\left. \begin{aligned} \frac{v_a}{R\zeta_0} &= \frac{1}{4} \frac{r}{R} + \frac{1}{2} K_1\left(\frac{R}{\lambda}\right) I_1\left(\frac{r}{\lambda}\right) \\ \frac{v_b}{R\zeta_0} &= \frac{1}{4} \frac{r}{R} - \frac{1}{2} K_1\left(\frac{R}{\lambda}\right) K_1\left(\frac{r}{\lambda}\right) \end{aligned} \right\} r < R, \\ \left. \begin{aligned} \frac{v_a}{R\zeta_0} &= \frac{1}{4} \frac{R}{r} + \frac{1}{2} I_1\left(\frac{R}{\lambda}\right) K_1\left(\frac{r}{\lambda}\right) \\ \frac{v_b}{R\zeta_0} &= \frac{1}{4} \frac{R}{r} - \frac{1}{2} I_1\left(\frac{R}{\lambda}\right) K_1\left(\frac{r}{\lambda}\right) \end{aligned} \right\} r > R. \end{aligned} \quad (6)$$

A vortex in the top layer displaces the density interface such that

$$\frac{\eta_2}{H} = \begin{cases} 1 + \frac{\zeta_0}{f} \left[1 - \frac{R}{\lambda} K_1\left(\frac{R}{\lambda}\right) I_0\left(\frac{r}{\lambda}\right) \right], & r < R, \\ 1 + \frac{\zeta_0 R}{f \lambda} I_1\left(\frac{R}{\lambda}\right) K_0\left(\frac{r}{\lambda}\right), & r > R. \end{cases} \quad (7)$$

In (6) the velocities are normalized by the velocity $R\zeta_0$ (rather than the alternative scale $\lambda\zeta_0$) as this is the correct scale for the maximum azimuthal velocity in the vortex. It is also noteworthy that the shapes of the velocity profiles are not dependent upon the value of the vorticity (or potential vorticity) in the core. Thus a cyclone and an anticyclone with equal and opposite relative vorticities ζ_0 have equal and opposite velocities. In the limit $R/\lambda \rightarrow 0$, we have $I_1(R/\lambda) \rightarrow \frac{1}{2}R/\lambda$ and we recover, for $r > R$, the result for a point vortex (Hogg & Stommel 1985):

$$v = \frac{1}{2} \frac{s}{r} \left[1 \pm \frac{r}{\lambda} K_1\left(\frac{r}{\lambda}\right) \right], \quad (8)$$

where the positive sign is for the top layer, the negative sign for the bottom layer. The constant $s = \frac{1}{2}R^2\zeta_0$ is the vortex intensity, and the vortex strength is $2\pi s$. The intensity serves as a convenient (and only) multiplying constant in (6) for arbitrary values of R/λ also. The circulation Γ outside the core is a function of distance from the vortex centre except in the barotropic limit ($\lambda = 0$), where $\Gamma = \pi s$.

The velocity profiles (6) are plotted in figure 2 for three values of the ratio of core radius to Rossby radius. In the limit $\lambda/R \rightarrow 0$, where the influence of density gradients vanishes and the flow becomes independent of depth, the structure approaches a Rankine vortex:

$$v_a = v_b = \begin{cases} \frac{1}{2} \frac{s}{R^2} r, & r < R, \\ \frac{1}{2} \frac{s}{r}, & r > R. \end{cases} \quad (9)$$

At the opposite extreme, $\lambda/R \gg 1$, the maximum velocity at the edge of the core approaches $v_a = \frac{1}{2}R\zeta_0 = s/R$, twice that in (9). The upper layer velocity again decreases with radius as $v_a \sim r^{-1}$, but only over distances comparable with the core radius. Over the much greater distance λ there is now an additional decrease such that, at $r \gg \lambda$, v_a asymptotes to the barotropic velocity (9). In this strongly stratified regime the velocities are independent of depth at $r \gg \lambda$ and strongly baroclinic at $r < \lambda$. At $r < \lambda$ the bottom layer velocity is much smaller than v_a , and reaches a

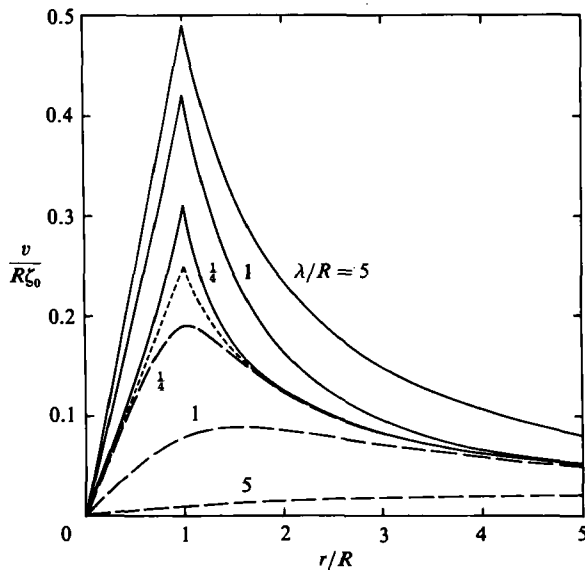


FIGURE 2. Examples of the azimuthal velocities (6) predicted for the quasi-geostrophic model in figure 1: —, top-layer velocities; ----, bottom-layer velocities; - · - ·, the barotropic limit $\lambda/R = 0$.

maximum value at $r \approx 1.1\lambda$. For intermediate values of the ratio λ/R , interfacial shear is always greatest at the outer edge of the core, but is smaller for smaller values of λ/R . At $\lambda/R \approx 1$ the top-layer velocity immediately outside the core decreases with increasing radius more rapidly than in either the unstratified or 'strongly stratified' cases. It must decrease to the barotropic profile within a distance comparable to R , and the induced far-field barotropic velocities are a smaller fraction of the maximum core velocity than is the case for $\lambda/R \ll 1$.

3.2. Structure of the laboratory vortices

Examples of the measured angular velocities θ about the vortex centre and linear velocities $v = r\theta$ for the unstratified case are shown in figure 3 (an anticyclone) and figure 4 (a cyclone). In all cases θ decreased monotonically with increasing radius, while the linear velocity passed through a maximum value at a radius of several centimetres. Beyond the velocity maximum the data are well described by the profile $v \sim r^{-1}$. The relative vorticity $\zeta = 2\theta + r d\theta/dr$ at small radii was not constant as assumed in the model of §3.1, and there was some rounding of the velocity peak. However, the structure of barotropic vortices was always close to that of a Rankine vortex, and remained essentially unchanged as the vorticity was dissipated in the bottom Ekman boundary layer. The Ekman number based on the kinematic viscosity ν and the background vorticity was $\nu/fH^2 \approx 10^{-5}$ (for $H = 20$ cm) or 3×10^{-6} (for $H = 40$ cm), implying an exponential timescale $H/(f\nu)^{1/2} \approx 140$ s (or 280 s) for dissipation. The smaller time corresponds to 23 rotation periods.

Between five and ten rotation periods after the forcing was turned off, anticyclones were characterized by maximum angular velocities (near $r = 0$) of $\theta \approx -0.5\Omega$, and cyclones by $\theta \approx 0.7\Omega$ to 1.2Ω . Since it is likely that $d\theta/dr = 0$ at $r = 0$, the maximum vorticity can be evaluated from $\zeta_0 \approx 2\theta(r = 0)$. For anticyclones we find $\zeta_0 \approx -0.5f$ and for cyclones $\zeta_0 \approx f$. On the other hand, at the radius of the velocity maximum, $dv/dr = 0$, $\zeta = \theta$ and the measurements give $|\theta| \approx 0.3\Omega$ for vortices of

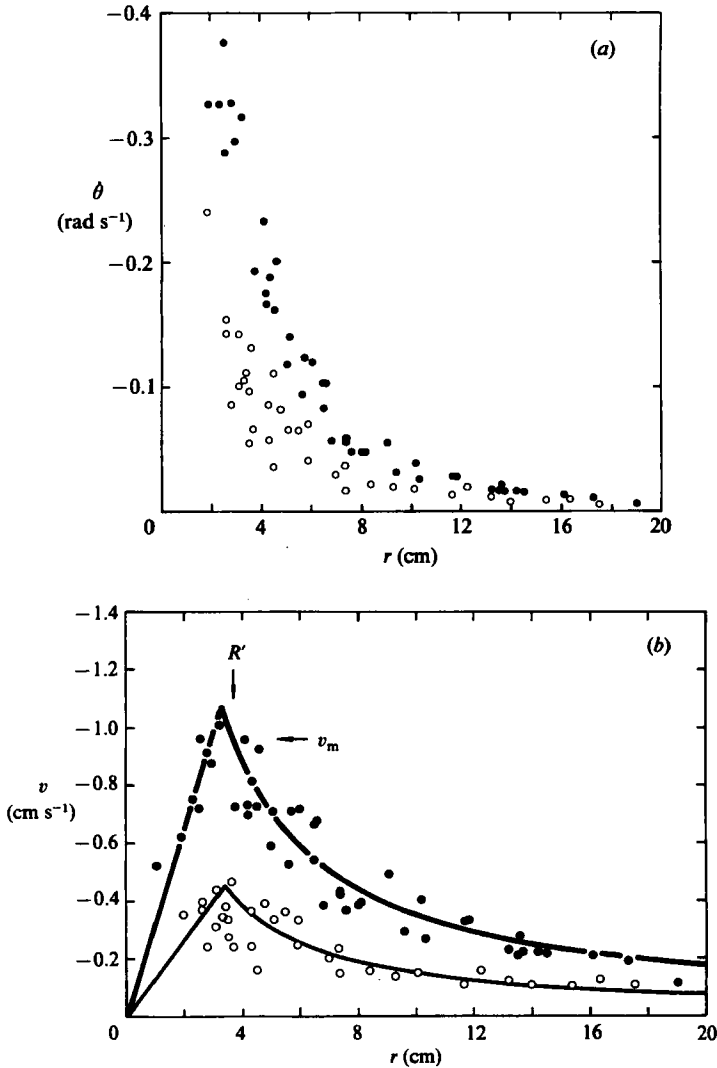


FIGURE 3. Measured angular velocities (a) and azimuthal velocities (b) in an unstratified anticyclonic vortex generated by a source. Measurements were taken at 10 rotation periods after forcing was turned off (●) and at $30T_D$ (○). Curves of the form $v = \frac{1}{2}s/r$ have been fitted to the data at $r > 4$ cm and give the vortex intensities $s = -7.0 \text{ cm}^2 \text{ s}^{-1}$ at $10T_D$, $s \approx -3.0 \text{ cm}^2 \text{ s}^{-1}$ at $30T_D$. Straight lines $v = ar$ are suggested for $r < 3$ cm. The core radius defined by (10) is 3.6 cm.

both signs. Hence flow near the edge of the core had a Rossby number $|\zeta|/f \approx 0.15$. This relatively small Rossby number is not surprising given that ζ vanishes a small distance beyond the radius of maximum velocity and that a discontinuity in vorticity cannot exist in the real flow. We also observed that small-scale shear instabilities always developed during the formation period of anticyclones. On breaking, these instabilities smeared horizontal vorticity gradients. From the above values for ζ_0 , the potential vorticity at the vortex centre was $\Pi_0 \approx 0.5f/H$ for anticyclones and $\Pi_0 \approx 2f/H$ for cyclones, where we recall that the fluid depth H in this unstratified case was constant after neglecting the very small slope ($< 1\%$) of the free surface.

For vortices in the top layer of a two-layer density stratification, the measured

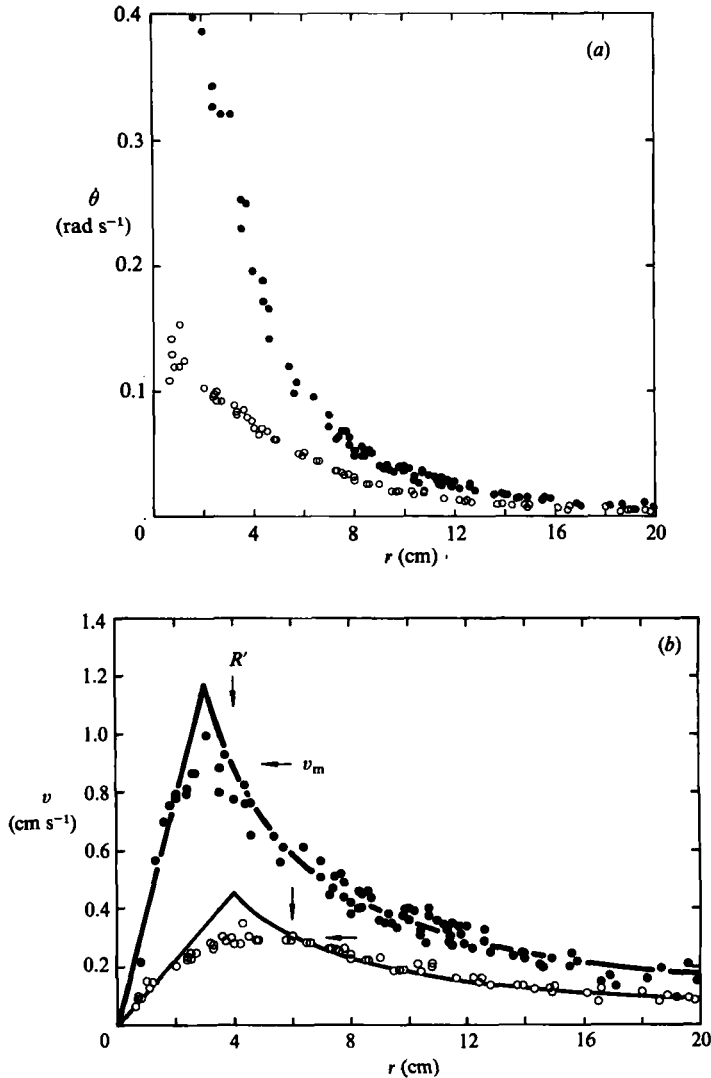


FIGURE 4. Angular velocities (a) and azimuthal velocities (b) measured in a barotropic cyclonic vortex generated by a sink. Data are for elapsed times of $10T_D$ (●) and $30T_D$ (○). Curves of the form $v = \frac{1}{2}s/r$ are fitted to the data for $r > 5$ cm and give the vortex intensities $s = 7.0 \text{ cm}^2 \text{ s}^{-1}$ at $10T_D$, $s = 3.6 \text{ cm}^2 \text{ s}^{-1}$ at $30T_D$. The core radius defined by (10) is 4.0 cm at $10T_D$ and 6.0 cm at $30T_D$.

velocity profiles (figure 5) show the same general structure in the top layer as found in the unstratified case. However, with the density difference chosen so as to give a Rossby radius $\lambda = 5$ cm, a clear deviation from the decay $v \sim r^{-1}$ occurred beyond the radius of maximum velocity. The more rapid decrease of velocity is well described by the solution (6) to the baroclinic model. Furthermore, the motion in the bottom layer was much smaller than that in the top layer at $r < 2\lambda$, while the flow became independent of depth at $r > 3\lambda$. A comparison can be made between the measured and model velocities (6) for the bottom layer by fitting the predicted form (6) for $v_a(r > R)$ to the data from the top layer using an estimate for the ratio R/λ , evaluating a multiplying constant (the vortex intensity), and then using that

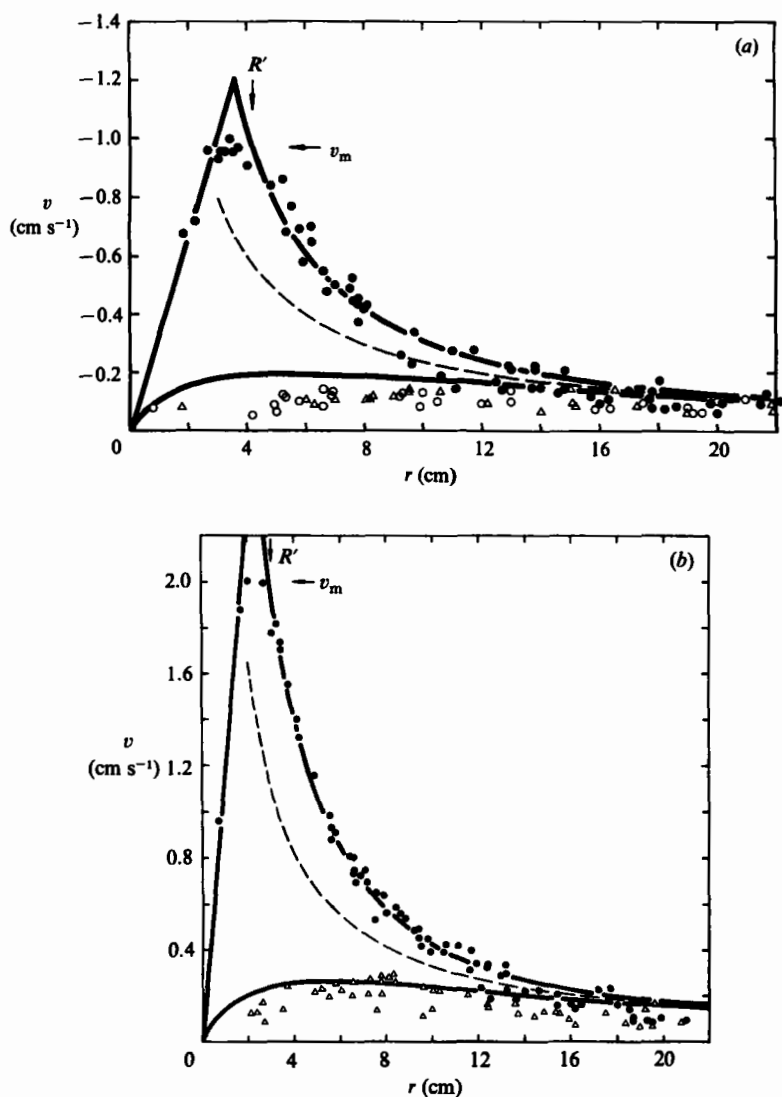


FIGURE 5. Azimuthal velocities measured in a two-layer anticyclone (a) and cyclone (b), each with $\lambda = 5 \text{ cm}$. Data are from the top layer at 9 rotation periods after generation (\bullet) and from the bottom layer at $6T_{\Omega}$ (\circ) and $12T_{\Omega}$ (\triangle). Solid curves are the profiles (6) predicted for two-layer vortices having piecewise uniform potential vorticity in the top layer. Their fit to the data gives, in these examples, the vortex intensities $s = -4.8 \text{ cm}^2 \text{ s}^{-1}$ and $s = 6.6 \text{ cm}^2 \text{ s}^{-1}$. Broken lines are the reference curves $v = s/2r$. Core radii defined by (10) are 4.2 cm in (a) and 3.0 cm in (b).

constant to compute the bottom-layer velocity v_b . The measured bottom layer velocities are modelled satisfactorily although they were slightly smaller than those predicted. The discrepancy is possibly a result of bottom friction and the finite interface thickness.

The maximum velocities and vorticities measured in top-layer cyclones were significantly larger than those in unstratified cyclones and in all anticyclones. Stretching of fluid columns provides a greater capacity for creation of relative vorticity than does compression of columns, and the greater vorticity in cyclones is

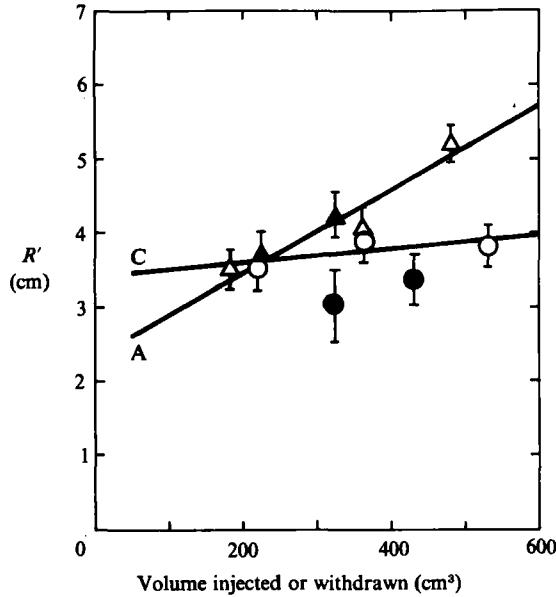


FIGURE 6. The core radius for the laboratory vortices after 5–10 rotation periods had elapsed as a function of the forcing applied during a 30 s period: \circ , barotropic cyclones; \bullet , two-layer cyclones with $\lambda = 5$ cm; \triangle , barotropic anticyclones; \blacktriangle , two-layer anticyclones with $\lambda = 5$ cm. The straight lines show a fit by eye to data for vortices of each sign.

rapidly dissipated in the unstratified case by a bottom Ekman layer. The appropriate timescale for the dissipation of the large initial vorticity is $H/(\zeta\nu)^{\frac{1}{2}}$ and is shorter than that based on the background vorticity. Dissipation of vorticity was slowest for the top-layer vortices, which were insulated from the rigid bottom by density gradients.

The choice of lengthscale used to describe the size of the region of anomalous potential vorticity is somewhat arbitrary. A fitting to the measured velocities of the model profiles assuming piecewise uniform potential vorticity suggests that the core radius R be defined as the radius at which the curves for $r \geq R$ intersect (as seen in figures 3–5). On the other hand, interactions between vortices and consequent advective perturbation of the axisymmetric potential-vorticity distribution can be expected to be dependent upon those potential-vorticity differences that are farthest from the vortex centre. A more relevant core radius is therefore assumed to be that at which the potential vorticity deviates significantly from its constant value outside the core. Hence we choose the well-defined radius R' at which the velocity v_a predicted for a uniform potential vorticity outside the core is equal to the maximum observed velocity v_m . For unstratified vortices (9) the core radius becomes $R' = \frac{1}{2}s/v_m = \Gamma/2\pi v_m$. For general baroclinic vortices

$$R' = \frac{1}{2} \frac{s}{v_m} \left[1 + 2I_1 \left(\frac{R}{\lambda} \right) K_1 \left(\frac{R'}{\lambda} \right) \right]. \quad (10)$$

In practice, as shown in figure 5, R' is very close to the radius at which the measured velocity profile meets that expected for a point vortex of the same strength.

The detailed velocity measurements for a number of isolated vortices were used to establish a calibration between vortex strength, core radius and flow rate through sources and sinks. The results for vortex intensity were given in Griffiths & Hopfinger

(1986) and showed that the intensity was proportional to the volume of water injected or withdrawn. The core radius evaluated between five and ten rotation periods after generation is given in figure 6. Anticyclone cores were larger for greater flow rates. The radii of cyclone cores varied little, presumably because R' was determined largely by the dimensions of the sink and by subsequent Ekman pumping. Indeed, the core radius for cyclones increased with time (see figure 4) as fluid was pumped into the centre via bottom or surface Ekman layers and fluid having anomalous vorticity was displaced outward. Top-layer cyclones, which spin down more slowly, therefore had slightly smaller core radii after five to ten rotation periods than did barotropic cyclones. The radius of anticyclones showed no definite change during spin-up. In the following discussion of vortex interactions we characterize each anticyclone and each top-layer cyclone by the strength and core radius expected five to ten rotation periods after their forcing was turned off. Dissipation of intensities is not of primary importance as vortex strengths are compared only to those of other similar vortices generated at the same time. For cyclones in contact with the bottom an increase of the core radius over tens of rotation periods needs to be taken into account as this lengthscale will be compared with the distance between vortices.

4. Coalescing of unstratified vortices

4.1. Two identical anticyclones

The behaviour of cyclonic and anticyclonic pairs in an ideal fluid is expected to be identical. However, we observed some differences which will be attributed to viscous effects, and therefore discuss the two cases individually.

When two identical anticyclones were generated in an unstratified tank they began to orbit clockwise around their mutual centre of vorticity in the manner expected for the advection of each vortex by the velocity field of the other. If the distance between sources was sufficiently small the vortices eventually coalesced to form a single anticyclonic vortex. If the distance was sufficiently large the anticyclones did not coalesce and often appeared to move farther apart. Thus there appears to be a critical distance d_* below which the two-vortex configuration was unstable and above which it was stable. In a sequence of thirteen experiments using the same forcing flow rate, the critical separation was 13 cm. For $d = 12.5$ cm the vortices coalesced, while for $d = 13.5$ cm they did not merge. If the distance is normalized by the core radius $R' = 3.9$ cm the critical condition can be written as $d_*/R' = 3.3 \pm 0.2$, where the uncertainty is due to uncertainties in both d_* and R' .

In cases where merging took place, dye revealed that the flow in each vortex became non-axisymmetric just prior to coalescing. A cusp developed on each vortex, giving them the appearance of the corotating V-shapes which Saffman & Szeto (1980) found as equilibrium solutions to the two-dimensional Euler equations, and which are unstable in numerical simulations (Overman & Zabusky 1982; Dritschel 1985). Naturally, we must be cautious in identifying the formation of cusps in the dyed water with a specific stage in the interaction of vortices, or even with unstable configurations. The V-shape occurred in a streamline whose radius was slightly less than half the distance between vortex centres and its appearance may simply imply that the vortices had moved sufficiently close together for the dyed portion of the vortex to be perturbed, the cusps previously existing at larger radii. On the other hand, the edge of the dye was, in most cases, close to the edge of the region of anomalous vorticity, so that the visible cusps indicated a distortion of the previously circular vortex cores. As the cusps grew they met each other and proceeded to be

drawn out around the opposite vortex. That is, dyed fluid from each vortex flowed around the outer edge of the dyed region of the opposite vortex. If amalgamation proceeded, two 'spiral arms' extended backward (anticlockwise) from the antipodes of the vortices. In the same manner as shown by numerical simulations (Christiansen 1973; Overman & Zabusky 1982) the combined structure passed through an elliptical shape (with axes lengths roughly 2:1) in which water from each vortex was confined to one end of an ellipse. However, the experiments showed that this coalition, the new vortex, rapidly became circular and contained two entwined spirals. The double-spiral structure was similar to that observed after pairing of vortices in mixing layers.

If the initial separation was close to the critical value, oscillations were often seen and the formation of cusps did not always herald coalescing. Vortices could interact and exchange some dyed water, but then move apart and become circular again. If $d \gtrsim d_*$, there was no further close interaction. If $d \lesssim d_*$, a second close interaction followed and led to complete amalgamation. Oscillations were also noted in the earlier numerical calculations.

The merging of vortices occurred after elapsed times of order 1–20 rotation periods, with larger initial separations giving longer times. An appropriate timescale for interactions is the period for the advection of vortices around their mutual centre of vorticity. This orbital period for barotropic vortices is $2\pi d^2/s$. In the experiments, a conveniently identifiable time that characterized coalescence was the elapsed time t_* at which the cusps began to be advected past each other (see figure 7*b*) immediately prior to merging. When normalized by the orbital period the elapsed time was of order $t_* s/2\pi d^2 \sim 10^{-1}$. Large separation distances tended to give larger dimensionless times, although this result was far from clear and reproducible.

4.2. *Two identical cyclones*

Cyclonic vortices in an unstratified tank coalesced in the same manner, qualitatively, as did anticyclones. However, in a sequence of sixteen experiments no stability boundary was found for cyclones and almost all pairs eventually coalesced. Large separations could not be tested as sidewall effects would have been comparable with the influence of one vortex on the other, and because the timescale for interactions would have been much larger than the spin-down timescale.

Photographs of the interaction of two cyclones with $d/R' \approx 4.5$ are shown in figure 7 (Plate 1). The second frame was taken close to the time t_* at which we judged merging to begin. In this case $t_* \approx 30T_\Omega$ or $t_* s/2\pi d^2 \approx 0.6$. Development of cusps, early exchange of dyed water, formation of two outer spiral arms, and final spiral structure of the coalition can be seen. In this example, the entwined spirals are not symmetric, indicating a small difference in the strengths of the two original vortices.

The dimensional time t_* for coalescing increased rapidly with initial separation distance, reflecting in part the squared dependence of the orbital period on the separation distance. However, even the dimensionless time $t_* \Gamma/2\pi^2 d^2$ increased with distance (figure 8). The trend in merging time alone could be attributed to the reduction of the vortex strength and increase of the orbital period due to dissipation, but this does not explain why cyclones coalesce from distances much larger than the critical value for anticyclones. One possible explanation for the apparent absence (or large size) of a critical separation distance is that bottom friction causes the core radius of cyclones to increase with time. Thus any given (and unstable) value of the ratio d/R' will eventually be exceeded and the time taken to enlarge the core must be added to the elapsed time before merging.

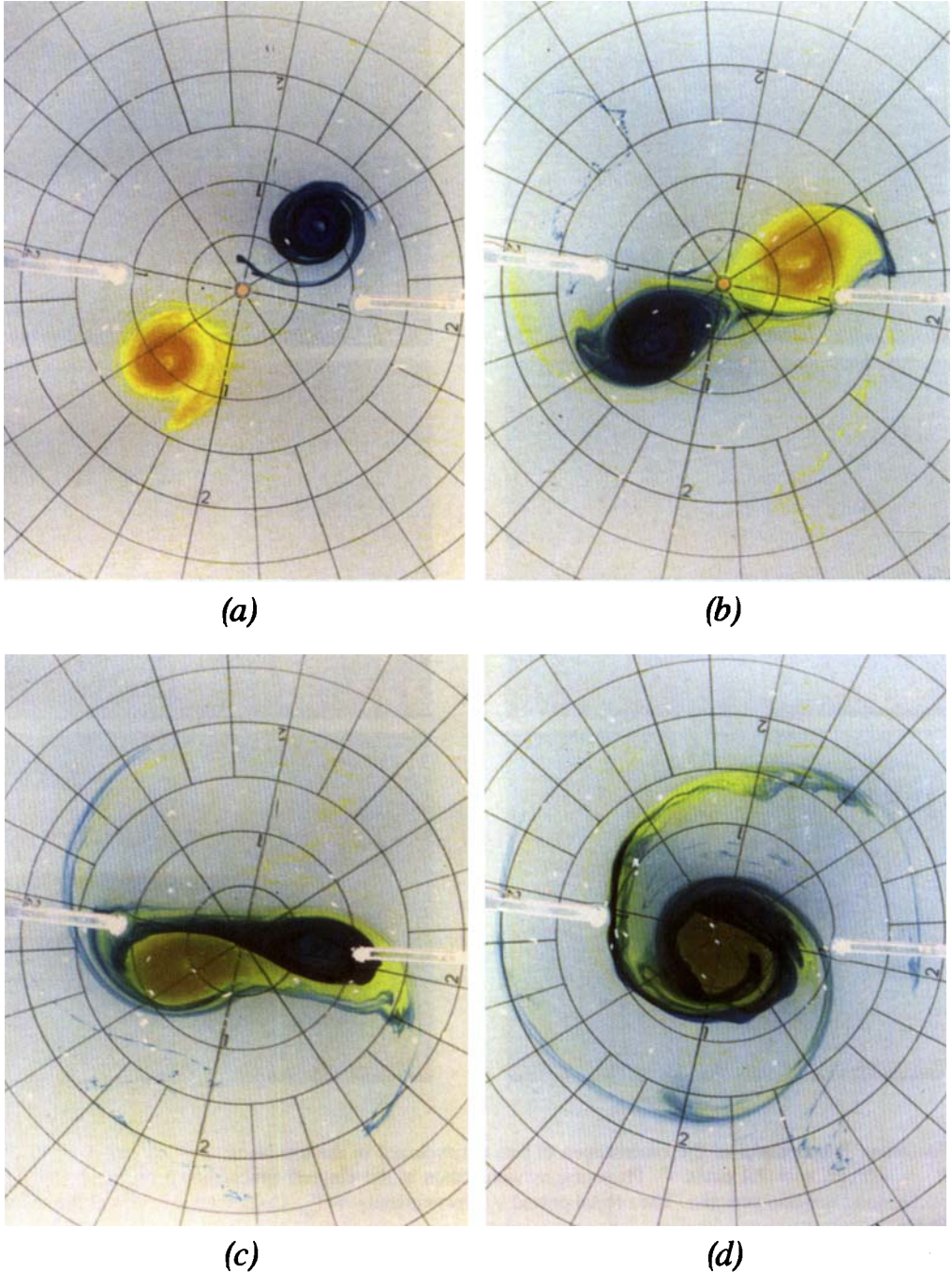


FIGURE 7. Photographs showing the coalescence of two unstratified cyclonic vortices. The initial separation is 20 cm, $s \approx 9 \text{ cm}^2 \text{ s}^{-1}$, $R' \approx 4.4 \text{ cm}$ and the initial orbital period is $44T_\Omega$. Photographs were taken at (a) $10T_\Omega$, (b) $30T_\Omega$, (c) $40T_\Omega$ and (d) $50T_\Omega$ after forcing was turned off. Tank rotation was anticlockwise.

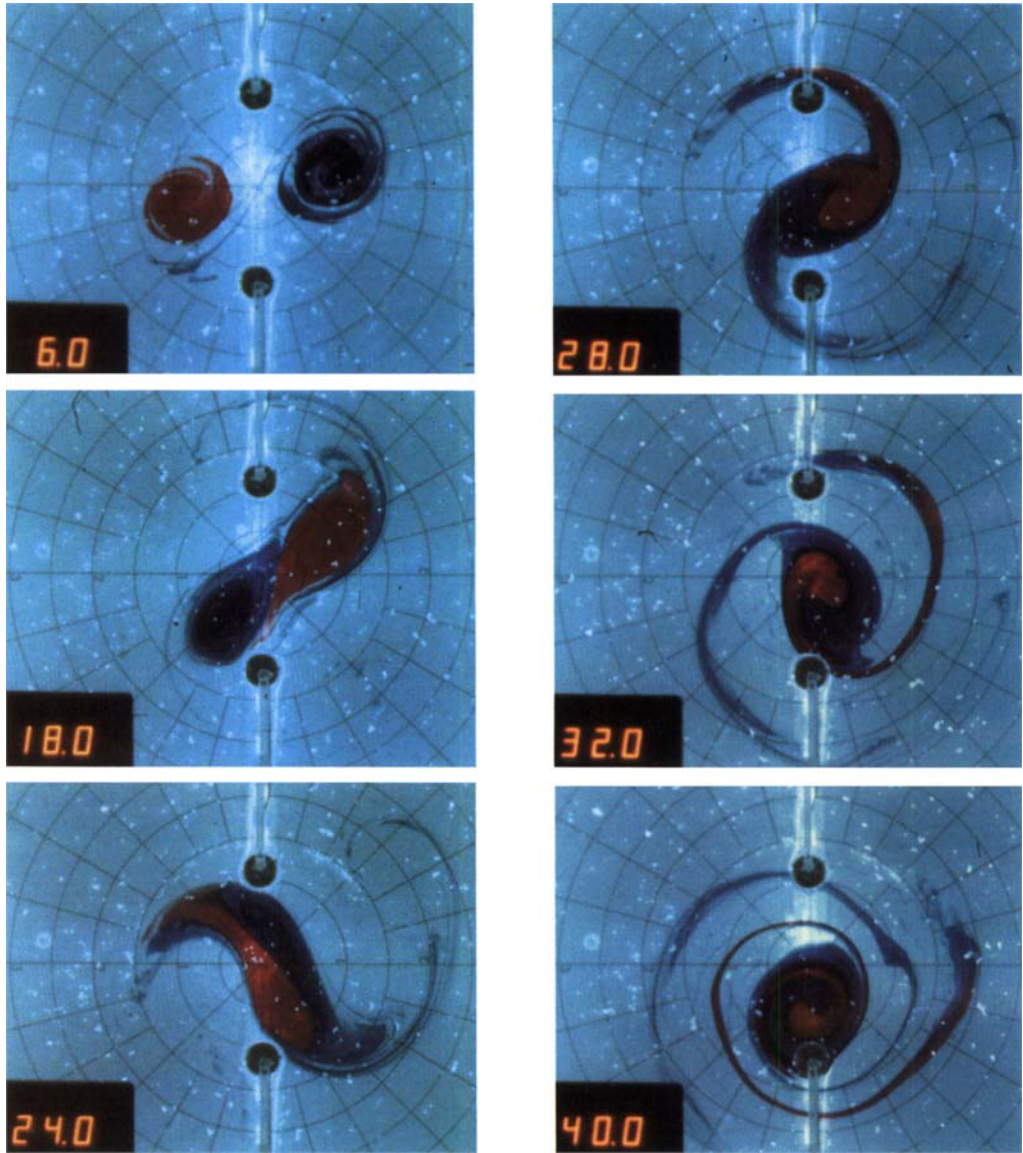


FIGURE 9. Photographs of the coalescence of two anticyclones in the top layer: $d = 18$ cm, $\lambda = 10$ cm, $R' = 4.0$ cm, $s = 7.4$ cm²s⁻¹. Photographs were taken at the elapsed times shown on the counter (in background rotation periods). The orbital period is approximately $44T_{\Omega}$. Coalescence begins at the second frame.

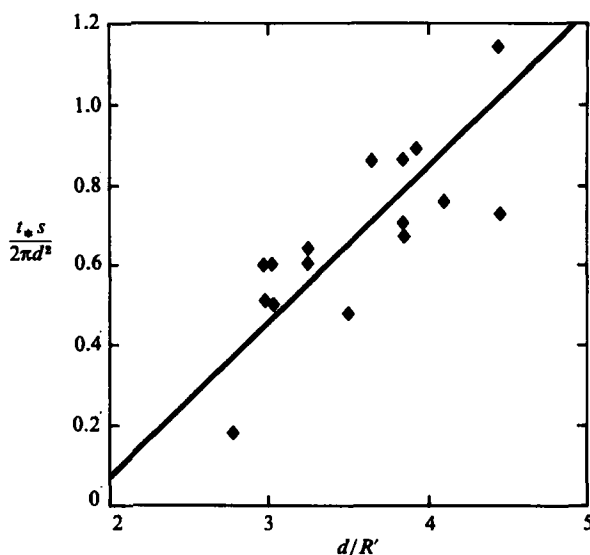


FIGURE 8. The dimensionless time elapsed before barotropic cyclones developed overlapping cusps and began to coalesce. Merging takes longer for greater separation distances.

A tendency for cyclones to attract each other was observed in early laboratory experiments (Fujiwhara 1913, 1923), where it was attributed to the convergence in the bottom friction layer. The convergence was thought to provide an attractive force between the cyclones. While this effect may play a minor role in our experiments, we note that convergence occurs only in a boundary layer which is 10^{-1} cm thick. Furthermore, the timescale for enlargement of the cyclonic core radius is given by the spin-down time (which in turn is only slightly greater than the merging times observed for anticyclones). In fact, calculation of the volume flux in a linear Ekman layer shows that the core radius of a cyclone should double in 30–100 rotation periods. Direct measurements show that the core radius increased by a factor of about 1.7 in the 25 rotation periods between $5T_\Omega$ and $30T_\Omega$ after generation. We conclude that dissipation leads to coalescing of (unforced) cyclones by enlarging the core to a radius at which a critical value of d/R' (possibly $d_*/R' \sim 3$) is exceeded. Existence of an absolute stability boundary at a large separation distance above which Ekman pumping does not lead to coalescing cannot be ruled out and experiments with much smaller Ekman numbers are needed.

5. Coalescing of baroclinic vortices

Density stratification can modify interactions between vortices through the effects of the baroclinic component of the velocity field and through the direct influence of buoyancy forces. Buoyancy forces oppose the increase in potential energy of the flow which must occur, in the absence of sufficient dissipation, as vortices of the same sign and at the same density level approach or coalesce (Hogg & Stommel 1985).

Two vortices (of either sign) generated in the top layer of a two-layer stratification coalesced whenever the distance between sources was less than a critical value, but did not merge from larger distances. Figure 9 (Plate 2) shows photographs of an experiment with $\lambda/R' = 2.5$ and $d/R' = 4.5$, in which the two identical anticyclones coalesced after $t_* \approx 5T_\Omega$ (second frame of figure 9) or $t_* s / 2\pi d^2 \approx 0.34$. In all cases,

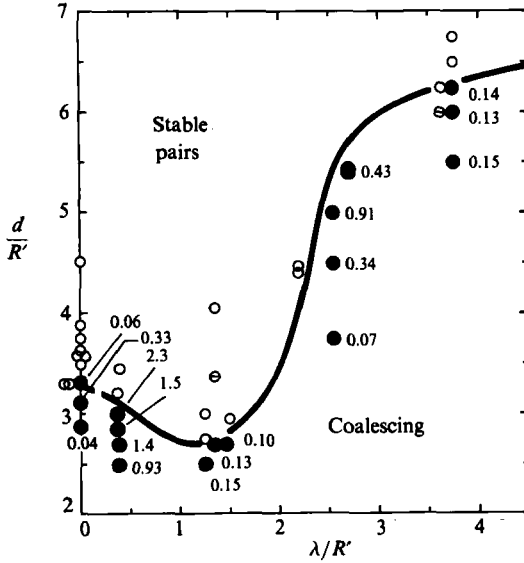


FIGURE 10. A classification of pairs of identical anticyclonic vortices as unstable (●), stable (○), or uncertain (⊖) defines a stability boundary (—). Stable pairs did not coalesce, unstable pairs did coalesce. Results for unstratified anticyclones are shown at the limit $\lambda = 0$, and appear to define a continuous limit for the stability boundary. However, the curve is not continued because baroclinic instability is likely to influence behaviour at small λ/R' . Elapsed dimensionless times before merging are shown for each pair.

the qualitative appearance of the interacting vortices and their union was similar to that already described for barotropic vortices, except that motion was independent of depth only within each layer and that their isolation from bottom friction allowed the top-layer vortices to remain active for more than 60 tank rotation periods. We note the formation of cusps and detrainment of two spiral arms. As in the unstratified case, baroclinic vortex pairs with separation distances close to the critical value experienced oscillations in which the vortices moved closer together, developed cusps, exchanged some dyed water, and separated again. However, the conditions under which vortices combined depended upon the Rossby radius.

Our results for symmetric anticyclonic pairs are summarized in figure 10, where the observations for unstratified anticyclones are included at the limit $\lambda = 0$. Unstable conditions, under which identical anticyclones coalesced, can be separated by a smooth curve from stable conditions, under which the vortices moved apart for an indefinite time. This curve will be referred to as the stability boundary. Beginning at $\lambda = 0$, where the critical distance is $d_*/R' \approx 3.3$, the stability boundary falls to slightly smaller values of the dimensionless separation with increasing Rossby radius, until it reaches a minimum of $d_*/R' \approx 2.7 \pm 0.1$ at $\lambda/R' \approx 1$. For Rossby radii greater than the core radius the critical distance increases rapidly with Rossby radius and reaches $d_*/R' \approx 6.3 \pm 0.3$ at $\lambda/R' = 4$. At this point the stability boundary might also be written as $d_* \approx 1.6\lambda$. Thus anticyclones coalesce from much greater distances when the Rossby radius is large compared with the core radius. In other words, the Rossby radius becomes the dominant horizontal lengthscale influencing vortex interactions.

The dimensionless times $t_* s/2\pi d^2$, where t_* is the time elapsed before coalescence as defined in §4, are given beside the data points in figure 10. The orbital periods

for the baroclinic pairs were approximately equal to $2\pi d^2/s$ since the distance d was always larger than one Rossby radius, making the contribution from the baroclinic component of the velocity (6) small. The time t_* ranged from $2T_\Omega$ to $50T_\Omega$ and was often much greater than the times recorded for barotropic anticyclones. Complete amalgamation generally required a further period of order $10T_\Omega$. Overlapping of cusps generally occurred at $0.1 < t_* s/2\pi d^2 < 1$ and the data show a possible systematic dependence of the time upon proximity to the stability boundary. This dependence is clear in the experiments having $\lambda/R' \approx 0.38$ ($\lambda = 1.5$ cm), where dimensionless times were larger for separation distances close to the critical distance. It is noteworthy that the experiments with a small Rossby radius ($\lambda = 1.5$ cm) also gave merging times that were larger than those found under other conditions, with t_* extending up to $47T_\Omega$, or 2.3 orbital periods.

Pairs of identical *cyclonic* vortices generated by sinks in the top layer also revealed a critical separation above which vortices moved apart and below which they coalesced. In this case, of course, they orbited around the centre of vorticity in the anticlockwise direction. The stability boundary for baroclinic cyclones was very similar to that in figure 10, again having a minimum of $d_*/R' = 2.7 \pm 0.1$ at $\lambda/R' \approx 1$, a steep increase of d_* at $\lambda \gtrsim 2R'$ and reaching $d_*/R' \approx 6$ at $\lambda/R' = 4$. Times elapsed before merging were similar also. The approximate coincidence of stability boundaries for top-layer vortices of both signs lends support to our calibrations of core radius as a function of flow rates through the sources and sinks, and to the accuracy of the empirical boundary. The results for top-layer cyclones also support the hypothesis advanced in §4.2 that the apparent absence of a stability boundary for unstratified cyclones was a result of bottom friction rather than of the nature of cyclones.

6. Discussion of results

6.1. Conditions for coalescing

The excellent agreement between the critical distance $d_*/R' \approx 3.3$ found here for unstratified anticyclonic vortices and that given by earlier two-dimensional numerical simulations using the Euler equations ($d_*/R \approx 3.2$) suggests that the details of the vorticity distribution in the laboratory vortices had little effect on vortex interactions. The numerical models had piecewise uniform vorticity, while the laboratory flow had a smoothly varying vorticity in the core. The core radius R' in the real vortex was chosen as the radius of the outer edge of the region of anomalous vorticity.

A variation of the critical distance with Rossby radius when the stratification is weak ($\lambda/R' \lesssim 1$) reflects the influence of the baroclinic component of the velocity field induced by each vortex. Baroclinicity causes a more rapid decay of the azimuthal velocity with increasing radius, and this effect is greatest when the Rossby radius is equal to the core radius. Thus the ratio of top-layer velocity at $r = 3R$, say, to the maximum velocity (always at $r = R$) given by the model in §3 is 0.33 when $\lambda \ll R$ or $\lambda \gg R$, but only 0.23 when $\lambda = R$. Hence the advective distortion of a neighbouring vortex core is weakest when $\lambda \approx R$, where a pair of vortices is likely to be stable at separation distances slightly smaller than the critical value for $\lambda = 0$. The empirical stability boundary does indeed pass through a minimum near $\lambda = R$.

It is more difficult to explain the observed increase of the critical separation distance at large Rossby radii. Coalescing from large distances at $\lambda/R' > 2$ can only be attributed to the effects of the large horizontal lengthscale λ on the velocity field

induced in the top layer by each vortex. The flow induced in the bottom layer is unlikely to influence vortex interactions as potential vorticity, not relative vorticity, is the dynamically significant property of geostrophic flow. Although the bottom layer contained a velocity maximum at $r \sim \lambda$ (when $\lambda \gg R'$), this layer initially had a uniform potential vorticity. Dissipation could produce only very small differences in potential vorticity in the bottom layer (because the velocities there were small). Hence we conclude that the layer remained passive.

Our data are not sufficient to enable us to ascertain whether the stability boundary asymptotes to a constant value ($d_* \geq 7R'$) at $\lambda \gg R'$ or whether the critical distance continues to increase with increasing Rossby radius, perhaps as rapidly as $d_* \sim \lambda$. Which ever is the case, the coalescing of pairs of 'strongly stratified' vortices from large separation distances is a surprising result. In the absence of dissipation and in the limit $\lambda/R \gg 1$, the quasi-geostrophic model of §3 shows that the available potential energy associated with interface displacements must double when two identical vortices in the same layer are brought from infinity to coalesce into a single vortex (Hogg & Stommel 1985). In at least some of the experiments, merging of top-layer vortices began within times as short as $t_* \approx 2T_\Omega$ and was completed within as little as $5T_\Omega$, times much smaller than the spin-up timescale (at least $40T_\Omega$) for the top layer. Hence the rate of dissipation of kinetic energy in Ekman boundary layers (with consequent conversion of potential to kinetic energy in order to maintain geostrophic balance) is unlikely to have been sufficient to prevent an increase in potential energy during coalescence.

If we consider coalescence as a barotropic (shear-induced) instability then it is pertinent to note that other barotropic instabilities in stratified flows (e.g. Kelvin-Helmholtz instability) are known to increase the potential energy of the fluid. If such an energy transformation occurred during vortex merging, it would not therefore be unusual. On the other hand, it is possible that large horizontal velocity gradients produced during merging may lead to dissipation sufficient to avoid an increase in potential energy. This is shear-enhanced diffusion, in this case accompanying a cascade of enstrophy to small scales. The growth of two 'spiral arms' of core fluid, arms that are separated from the new combined core by bands of outer irrotational fluid, provides a likely site for alteration of the potential vorticity of the fluid thrown out into those arms. This dissipation is equivalent to a loss of volume from the core region and in the barotropic case is known to allow conservation of angular momentum. In the baroclinic case we speculate that the spiral arms not only conserve the angular momentum of the system, but might also allow coalescence to proceed without an increase in potential energy. Unfortunately, we were unable to determine whether the vertical displacement of the density interface increased during coalescence, as this would have been indicative of potential-energy changes. It is as well also to recall here Dritschel's (1985) result for the barotropic case: extremely small amounts of dissipation (measured as the ratio of the time t_M required for complete coalescence to the dissipation timescale τ , $t_M/\tau \ll 1$) can facilitate completion of transitions that could not occur in an ideal fluid. Hence the role of dissipation, both by Ekman layers on horizontal boundaries and by horizontal diffusion, in interactions of baroclinic vortices remains to be clarified.

Another possible mechanism for dissipation and alteration of potential vorticity during coalescence is proposed by Nof (1986). He suggests that internal bores (shock waves) may form at the noses of the tentacles of fluid which flow from each eddy and encircle the neighbouring eddy. Fluid in the tentacles initially possesses the anomalous potential vorticity of the vortex cores and forms a contrast with the

ambient fluid. If such bores are able to effect sufficient alteration of potential vorticity then coalescing would not require an increase in potential energy nor, in the case of isolated frontal eddies, an increase in the total energy of the flow. Nof (1986) suggests that internal bores occur during close interactions of isolated frontal eddies. However, it is clear from his analysis (and also from our laboratory observations) that fluid within the spiralling tentacles does not travel toward the nose of the tentacle. Hence very little of the vortex fluid can be expected to be processed by a bore. Furthermore, the details of the merging process as observed in our experiments with two-layer (non-isolated) vortices are so remarkably similar to those of the coalescence of unstratified, two-dimensional vortices that we are led to argue that internal bores (which cannot exist in the barotropic case) play no role in the interaction of baroclinic eddies. Indeed, it is unlikely that shocks can form even in our two-layer case, since depth perturbations were very small compared with the layer depth.

6.2. *Coalescing versus baroclinic instability*

While coalescing of vortices can be thought of as a barotropic instability (one which may conceivably increase the potential energy of the flow), it is known that individual baroclinic vortices will break-up under certain conditions as a result of baroclinic instability, a process which reduces the available potential energy. Baroclinic instability occurs when the horizontal lengthscale of the flow is large compared with the Rossby radius. For example, two-layer vortices generated by a small source of less dense water at the surface of a more dense solution break up into smaller structures when $\lambda/R < 10^{-1}$ (Griffiths & Linden 1981), where R is a core radius. Thus even if two stable vortices approached each other and coalesced according to the results presented above, the larger combined vortex would exceed this baroclinic stability criterion and break-up again when each of the original vortices satisfied $\lambda/R < 0.2$. While the criterion is only approximate, it serves to indicate that there may be a competition between the fusion of vortices having small Rossby radii or large core sizes, and fission of the vortex so produced. Indeed, such a competition forms a part of stratified geostrophic turbulence in which there is an energy cascade towards smaller horizontal wavenumbers and a blocking of this cascade at a wavenumber of order λ^{-1} by baroclinic instability. Coalescence of vortices is one mechanism by which energy can be transferred to larger scales, while baroclinic instability tends to place an upper bound on the scale of eddies and returns energy to a smaller scale.

The inevitable break-up of vortices at small values of λ/R' as a result of baroclinic instability leads to an uncertainty in our stability-boundary delineating conditions under which vortex pairs are stable to vortex merger (we have left a break in this curve at $\lambda/R' < 0.2$, figure 10). The timescale for merging ($\sim d^2/s$) is in general independent of that for growth of unstable baroclinic waves ($\sim 10f^{-1}$). Hence it might be possible for two vortices to completely coalesce before waves have time to grow and break the vortex apart. The stability boundary would then continue smoothly to the barotropic limit. However, fusion of laboratory vortices at $\lambda/R' \approx 0.38$ required tens of rotation periods, a result largely determined by the Rossby number of the flow, and similar timescales are expected for still smaller Rossby radii. These times are similar to or greater than those required for fission of the product vortex. Hence it is unlikely that fusion would occur at $\lambda/R' < 0.2$. We did not venture to explore these conditions in our experiments. Finally we note that baroclinic instability must give way to only barotropic shear instability close to the limit $\lambda/R \rightarrow 0$, where we find that amalgamated vortices are stable.

6.3. *Experiments with dissimilar vortices*

Only interactions of two identical vortices have been discussed so far. In some additional experiments, two vortices of the same sign were generated using different forcing flow rates during the usual 30 s forcing period. The resulting vortices were expected to have similar potential vorticities but different core radii and intensities. These unequal vortices coalesced from larger separation distances than did identical vortices, although the relationship between the ratio of intensities and critical distance was not explored in detail. When merging occurred the weaker vortex was always drawn out and wrapped around the outside of the stronger core. An interaction of two anticyclones with different intensities is shown in figure 11. Water originally in the top-layer core of the weaker vortex is eventually found in an annular volume surrounding the stronger core. The two unstratified cyclones shown coalescing in figure 7, although nominally of equal strength, also led to an asymmetric spiral pattern in the final stages of coalescence, suggesting that the vortex containing blue dye was very slightly weaker than that containing yellow dye.

Our observations for unequal pairs of both barotropic and baroclinic vortices are consistent with the behaviour found in numerical simulations for the two-dimensional, unstratified case. Overman & Zabusky (1982) described the asymmetric interaction as 'entrainment' of the region of greater vorticity density (the stronger vortex core) within the region of smaller vorticity density.

6.4. *Ocean eddies and tropical cyclones*

Among the most energetic of features in ocean circulation are the large warm-core and cold-core eddies formed from the intense western boundary currents. The eddies, or 'rings', are generated by baroclinic instability of the currents. They therefore have diameters that scale with the internal Rossby radius. The eddies lie in a density stratification that is often modelled as two layers – an upper layer approximately 200 m deep overlying a much deeper bottom layer. However, the interface is displaced downward by warm-core eddies to depths close to 500 m. The appropriate Rossby radius based on the depth of the eddies is about 30 km.

Hydrographic surveys of Gulf Stream warm-core rings (e.g. Olson *et al.* 1985) indicate that there is a maximum azimuthal velocity of approximately 0.6 ms^{-1} at a radius of 50 km. Warm anticyclonic eddies formed in the Tasman Sea by the East Australia Current tend to be somewhat larger, with maximum velocities between 1 and 2 ms^{-1} at a radius as large as 100 km (e.g. Andrews & Scully Power 1976; Nilsson & Cresswell 1980; Cresswell & Legeckis 1986). Taking the radius of maximum velocity as an estimate for the core radius R' , the ratio of Rossby radius to core radius for ocean eddies lies in the range $0.3 < \lambda/R' < 0.6$. The Rossby number $\zeta/f \approx -0.3$ is similar to that in our laboratory vortices. Assuming that the real density profiles do not greatly influence interactions between eddies, the experiments indicate that two ocean eddies will coalesce if their centres are brought to within three core radii. This critical distance will be about 150 km for Gulf Stream rings and up to 300 km for East Australia Current eddies.

A notable difference between the two-layer laboratory eddies and warm ocean eddies formed by frontal systems such as the Gulf Stream is that the latter eddies are much deeper than the ambient upper layer. Frontal eddies are therefore often modelled as vortices in which the density interface intersects the surface around their perimeter, confining the upper-layer water solely within the eddies (Flierl 1979). In order to observe the interaction of two such frontal eddies, we carried out experiments

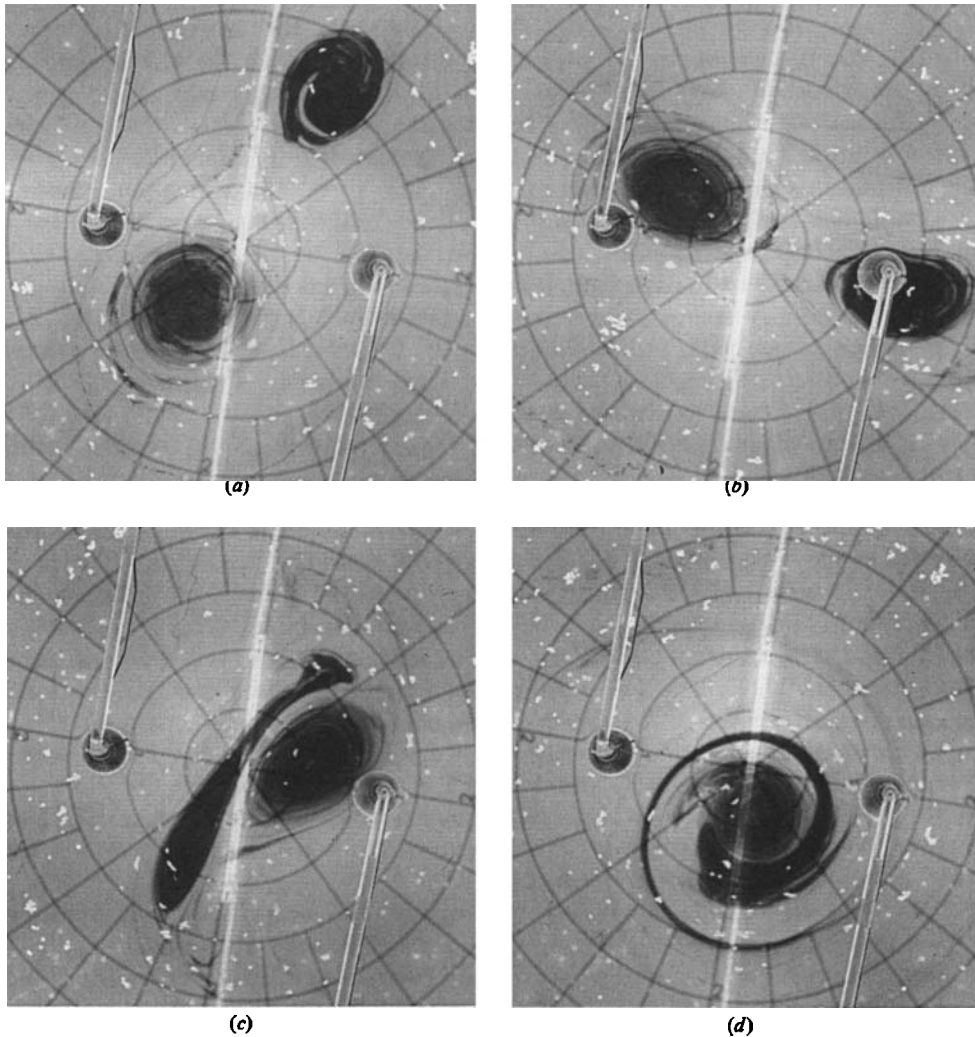


FIGURE 11. Photographs of the interaction between two baroclinic anticyclones of differing strengths. These were generated using differing source flow rates: $d = 20$ cm, $\lambda = 10$ cm, $\bar{R} \approx 3.7$ cm, $d/\bar{R} \approx 2.7$. The weaker vortex is drawn out and wrapped around the stronger. Photographs were taken after (a) 10, (b) 20, (c) 29 and (d) 40 rotation periods. As in all experiments, tank rotation was anticlockwise.

in which two anticyclones similar to those used by Griffiths & Linden (1981) were produced by injecting dyed less-dense water through two sources at the surface of a more-dense sugar solution. These vortices too coalesced whenever the sources were sufficiently close together, and interactions were qualitatively similar to those described in §§4 and 5. Although the depth of the top layer in these experiments vanished on the perimeter of the eddies, the eddies were not truly isolated because injection of the buoyant fluid caused divergence in the lower layer and consequent anticyclonic motion. Two frontal eddies therefore orbited around each other before their edges touched.

Although there are few observations that suggest that ocean eddies ever coalesce, an amalgamation of two warm eddies in the Tasman Sea was extensively documented

(Cresswell 1982; Cresswell & Legeckis 1986). In January 1981 eddies 'Leo' and 'Maria' came into close proximity. They rotated in the anticyclonic direction (anticlockwise in the southern hemisphere) about a point on the line joining their centres for about 20 days before coalescing into one stronger eddy. The reported drifter and satellite data can be used to estimate azimuthal water velocities within 'Leo' of $v_m \approx 0.7 \text{ ms}^{-1}$ at a radius of about 80 km during December 1980. Temperature sections indicate that this radius is close to that at which the maximum geostrophic velocity should exist. 'Maria' appeared slightly larger, with velocities of about 0.6 ms^{-1} at $R \approx 100 \text{ km}$, which is again close to the radius at which the geostrophic velocity estimated from temperature sections should be a maximum. In otherwise stationary surroundings these eddies should have rotated around their mutual centre of vorticity with a period of $4\pi d^2[1 + (d/\lambda)K_1(d/\lambda)]/(s_1 + s_2)$, where s_1 and s_2 are the vortex intensities. Since $\lambda/R \ll 1$, the intensities are given by $s \approx 2Rv_m$. When the eddies began to orbit each other their centres were 160 km apart, giving $d/\lambda \gg 1$ and an orbital period of about 16 days. Cresswell (1982) reports a slower motion through roughly 90° in 20 days, probably a result of the influence of the nearby continental shelf and other eddies.

The close interaction of 'Leo' and 'Maria' lasted for 20 days, a time consistent with the broad range of elapsed times (up to two orbital periods) found in the experiments with small Rossby radii. Furthermore, the separation distance $d = 160 \text{ km}$ gives $d/R' \approx 1.6\text{--}2.7$, placing the vortices below the stability boundary for coalescing. A small tongue of water from eddy 'Leo', the weaker of the two, was detected around the perimeter of 'Maria' (at $R \approx 90 \text{ km}$) a few days before the eddies coalesced. Such a feature was often seen in the experiments. After coalescence, the combined eddy was slightly more intense than either original vortex, with the water velocity reaching a maximum of approximately 1.4 ms^{-1} at a radius of 100 km. An additional complication in this event was that the original eddies contained waters of different densities. These water masses were later recognizable as two distinct layers overlying each other in the core of the combined eddy.

At the opposite extreme to barotropic vortices and baroclinic ocean eddies are intense atmospheric cyclones or hurricanes. Hurricanes often develop in pairs (Hoover 1961; Brand 1970) and rotate around each other. The individual hurricanes have small core radii ($R' \approx 10\text{--}80 \text{ km}$) and are embedded in the tropical atmosphere, which has a large internal Rossby radius ($\lambda \approx 800 \text{ km}$). Thus $\lambda/R' = 10\text{--}80$. Extrapolation of the empirical stability boundary for pairs of identical vortices to such large ratios of Rossby radius to core radius, although uncertain and neglectful of bottom friction, indicates that two hurricanes will coalesce from distances of at least $d_* \approx 7R'$. Bottom friction is likely to further increase the critical distance. Hence $d_* = 100\text{--}600 \text{ km}$ (depending on the core radius) is a lower limit for the critical separation distance. Since the observed orbital periods for hurricane pairs with separations close to 500 km, say, are between two and four days (Gryanik 1983), our experiments indicate the merging would take place within 10 hours of hurricane development. Such rapid coalescence is consistent with the almost complete absence of observations of hurricane pairs having separations of less than 400 km. Hurricane pairs having separations of less than 750 km are known to attract each other (Brand 1970) but owing to both the greater distance and effects of bottom friction are predicted to take much longer to merge, if they do so at all.

7. Conclusions

A pair of like geostrophic vortices generated by sources or sinks in a rotating fluid coalesce into a single vortex if the vortex centres are placed less than a critical distance apart. The critical distance for two identical barotropic vortices is equal to 3.3 core radii R' , where R' is the radius of the region of anomalous potential vorticity. This result is in excellent agreement with previous numerical simulations of the interaction of two-dimensional vortices having piecewise uniform vorticity in a non-rotating fluid. The background rotation in the experiments with no density gradients serves only to provide a convenient means of creating vortices in a well-controlled manner. Coriolis forces associated with the background rotation are balanced by a geostrophic component of the pressure gradient, leaving the flow to behave as it would in a non-rotating system. Furthermore, in appearance at least, the coalescence of an isolated pair of vortices is similar to the vortex 'pairing' observed in unstable shear layers. If the original vortices are identical the final union consists of two entwined spirals of fluid, each spiral containing water from one of the original vortices. If the original vortices are unequal, the water within the weaker vortex is wrapped around the core of the stronger vortex.

Additional effects due to Ekman pumping through Ekman layers on rigid boundaries perpendicular to the axes of vortices were observed for cyclone pairs. These effects are likely to be relevant also to vortices of *both* signs in contact with rigid boundaries in *non*-rotating systems. Cyclones, like all vortices in non-rotating flows, are spun down by Ekman pumping which, at the same time, causes the radius of the vortex core to enlarge. Our experiments show that such vortices coalesce from distances larger than the critical distance for inviscid vortices. Interactions of anticyclones are not significantly influenced by viscosity.

Baroclinic vortices too have a critical separation distance below which they coalesce, despite a potential-energy barrier. When the Rossby radius is close to one core radius the velocity decays more rapidly with radius in each vortex than it does in the barotropic limit, and vortices must be brought close together before they will coalesce. However, when the Rossby radius is greater than two core radii baroclinic vortices merge from much greater distances. The former case is relevant to ocean eddies, which are characterized by core radii larger than the Rossby radius. The ocean eddies should coalesce when $d < 3R'$, and this prediction is consistent with the behaviour observed in one event. However, it should be noted here that both our theoretical and laboratory models of baroclinic eddies give azimuthal velocities that decay with radius as $1/r$ at large distances from the vortex centre. Hence these are not isolated eddies, whereas warm-core eddies shed from major western boundary currents are often modelled as isolated structures (for which the velocity field decays more rapidly with radius). Such isolated eddies are likely to interact more weakly at distance and to experience a greater potential-energy barrier to coalescence. In our experiments, the development of two 'spiral arms' of core fluid conserves angular momentum and, through the detrainment of volume from the vortex cores (or equivalently by alteration of the potential vorticity of some core fluid), may also allow merging to continue without an increase of the potential energy.

Derek Corrigan is thanked for the construction of equipment and willing assistance in the laboratory. Ross Wylde-Browne is thanked for coping with endless photographs of coalescing vortices, for preparation of figures and for editing a movie. Karen Buckley is thanked for typing the manuscript. E. J. H. received a Visiting Fellowship from the Australian National University.

REFERENCES

- ANDREWS, J. C. & SCULLY POWER, P. 1976 The structure of an East Australian Current anticyclonic eddy. *J. Phys. Oceanogr.* **27**, 405–415.
- AREF, H. 1983 Integrable, chaotic, and turbulent vortex motion in two-dimensional flows. *Ann. Rev. Fluid Mech.* **15**, 345–389.
- BRAND, S. 1970 Interaction of binary tropical cyclones of the western North Pacific Ocean. *J. Appl. Met.* **9**, 433–441.
- BROWN, A. L. & ROSHKO, A. 1974 On density effects and large structure in turbulent mixing layers. *J. Fluid Mech.* **64**, 775–816.
- CHRISTIANSEN, J. P. 1973 Numerical simulations of hydrodynamics by the method of point vortices. *J. Comput. Phys.* **13**, 363–379.
- CHRISTIANSEN, J. P. & ZABUSKY, N. J. 1973 Instability, coalescence and fission of finite-area vortex structures. *J. Fluid Mech.* **61**, 219–243.
- CRESSWELL, G. R. 1982 The coalescence of two East Australia Current warm-core eddies. *Science* **215**, 161–164.
- CRESSWELL, G. R. & LEHECKIS, R. 1986 Eddies off southeastern Australia, 1980/81. *Deep-Sea Res.* **33**, 1527.
- DRITSCHEL, D. G. 1985 The stability and energetics of corotating uniform vortices. *J. Fluid Mech.* **157**, 95–134.
- FLIERL, G. R. 1979 A simple model for the structure of warm and cold core rings. *J. Geophys. Res.* **84**, 781–785.
- FUJIWHARA, S. 1913 Short note on the behaviour of two vortices. *Proc. Physico-Math. Soc. Japan*, Third Series **13**, 106–110.
- FUJIWHARA, S. 1923 On the growth and decay of vortical systems. *Q. J. R. Met. Soc.* **49**, 75–104.
- GILL, A. E. & GRIFFITHS, R. W. 1981 Why should two anticyclonic eddies merge? In Ocean Modelling, 41. Unpublished manuscript.
- GRIFFITHS, R. W. & HOPFINGER, E. J. 1986 Experiments with baroclinic vortex pairs in a rotating fluid. *J. Fluid Mech.* **173**, 501–518.
- GRIFFITHS, R. W. & LINDEN, P. F. 1981 The instability of vortices in a rotating, stratified fluid. *J. Fluid Mech.* **105**, 283–316.
- GRIFFITHS, R. W. & LINDEN, P. F. 1985 Intermittent baroclinic instability and fluctuations in geophysical circulations. *Nature* **316**, 801–803.
- GRYANIK, V. M. 1983 Dynamics of singular geostrophic vortices in a two-level model of the atmosphere (or ocean). *Izv. Akad. Nauk. SSSR Atmos. Oceanic Phys.* **19**, 171–179.
- HOGG, N. G. & STOMMEL, H. M. 1985 The heton, an elementary interaction between discrete baroclinic geostrophic vortices and its implications concerning eddy heat-flow. *Proc. R. Soc. Lond. A* **397**, 1–20.
- HOOVER, E. W. 1961 Relative motion of hurricane pairs. *Mon. Weath. Rev.* **89**, 251–255.
- NILSSON, C. S. & CRESSWELL, G. R. 1980 The formation and evolution of East Australia Current warm-core eddies. *Prog. Oceanogr.* **9**, 133–183.
- NOF, D. 1986 The coalescence of isolated eddies. *J. Phys. Oceanogr.* (submitted).
- OLSON, D. B., SCHMITT, R. W., KENNELLY, M. & JOYCE, T. M. 1985 A two-layer diagnostic model of the long-term physical evolution of warm-core ring 82B. *J. Geophys. Res.* **90**, 8813–8822.
- OVERMAN, E. A. & ZABUSKY, N. J. 1982 Evolution and merger of isolated vortex structures. *Phys. Fluids* **25**, 1297–1305.
- PEDLOSKY, J. 1979 *Geophysical Fluid Dynamics*. Springer. 624 pp.
- PIERREHUMBERT, R. T. & WIDNALL, S. E. 1981 The structure of organized vortices in a free shear layer. *J. Fluid Mech.* **102**, 301–313.
- ROSSOW, V. J. 1977 Convective merging of vortex cores in lift-generated wakes. *J. Aircraft* **14**, 283–290.

- SAFFMAN, P. G. & SZETO, R. 1980 Equilibrium shapes of a pair of equal uniform vortices. *Phys. Fluids* **23**, 2339–2342.
- THORPE, S. A. 1973 Experiments on instability and turbulence in a stratified shear flow. *J. Fluid Mech.* **61**, 731–751.
- WINANT, C. D. & BROWAND, F. K. 1974 Vortex pairing: a mechanism of turbulent mixing-layer growth at moderate Reynolds number. *J. Fluid Mech.* **63**, 237–255.